

# Vacuum Ultraviolet Smoothing of Nanometer-Scale Asperities of Poly(methyl methacrylate) Surface

R. V. Lapshin<sup>a, b</sup>, A. P. Alekhin<sup>a, b</sup>, A. G. Kirilenko<sup>a</sup>, S. L. Odintsov<sup>a</sup>, and V. A. Krotkov<sup>a</sup>

<sup>a</sup>State Scientific Center of Russian Federation, Institute of Physical Problems named after F. V. Lukin, Zelenograd, 124460 Russia

e-mail: rlapshin@yahoo.com, rlapshin@gmail.com

<sup>b</sup>Moscow Institute of Physics and Technology, Dolgoprudnyi, Moscow Region, 141700 Russia

Received June 4, 2009

**Abstract**—Smoothing of the nanometer-scale asperities of a poly(methyl methacrylate) (PMMA) film using vacuum ultraviolet (VUV) with the wavelength  $\lambda = 123.6$  nm was studied. The exposure time and the residual air pressure in a working chamber were varied during the process of VUV treatment. A nanostructured surface of PMMA film is used as a sample to be exposed. The nanostructured surface of the PMMA film was obtained by treating the initially smooth spin-coated film in oxygen radio-frequency plasma. The degree of VUV exposure is estimated using changes in the morphology and roughness of the nanostructured surface, which were determined by atomic-force microscopy (AFM). Recognition of morphological surface features on the AFM-images and determination of main geometrical characteristics of these features are performed by using virtual feature-oriented scanning method. It is discovered by morphology and Fourier spectra that the nanostructured surface of the PMMA film is partially ordered. The developed VUV smoothing procedure can be used to treat the electron-beam, UV, and X-ray sensitive PMMA resists, PMMA elements of micro-electromechanical systems, biomedical PMMA implants, as well as to certify nanotechnological equipment incorporating UV radiation sources.

DOI: 10.1134/S1027451010010015

## INTRODUCTION

At present, poly(methyl methacrylate) (PMMA) is widely used as electron-beam, UV, and X-ray sensitive resists in micro- and nanoelectronics [1–3], a thermoplastic material in nanoimprinting [4–7], a construction material in microfluidic devices [4, 8–12] and microelectromechanical systems (MEMS) [6, 13], and a material for artificial organs in transplantology [14].

UV treatment at a low pressure of a working gas makes it possible to directly change physicochemical properties of the PMMA surface without changing the properties of the polymer material in bulk and without heating the polymer significantly [15, 16]. In particular, by using UV treatment, film thickness and PMMA surface roughness can be decreased in the nanometer range. The minimum size of a nanoelement fabricated by lithographic methods depends considerably on the film thickness and the surface roughness of a PMMA resist [1–4]. Roughness in the nanometer range affects the performance of rubbing MEMS elements considerably and governs the biocompatible properties of implant surfaces significantly [14]. Thus, the application of UV treatment methods changing the PMMA surface roughness in the nanometer range is of great practical interest today.

In addition, to estimate the operating characteristics of the technological equipment designed for a

photostimulated modification of the polymer surface in the nanometer range, test objects that are convenient in use and contain nanoscale features, are required. A test object that is easily fabricated, measured, and analyzed is proposed in this paper. It is a PMMA surface nanostructured in oxygen radio-frequency (RF) plasma.

## EQUIPMENT, SAMPLES, TREATMENT PROCESSES, AND INVESTIGATION METHODS

VUV PMMA treatment was performed using the laboratory polymer modification system PMS-2. This system was developed and produced in the Institute of Physical Problems named after F. V. Lukin, the State Scientific Center of Russian Federation. The functional scheme of the system is shown in Fig. 1.

Using krypton resonance lamps as UV radiation sources enables us to produce cheap and compact VUV treatment devices. Two KrR-3 krypton lamps (State Optical Institute) with the radiation wavelength  $\lambda = 123.6$  nm and intensity of approximately  $6.6 \times 10^{-3} \text{ J cm}^{-2} \text{ s}^{-1}$  are used in the PMS-2 system. The exit windows of these lamps are made of  $\text{MgF}_2$ , which transmits radiation with the wavelength  $\lambda < 150$  nm. The distance between the krypton lamp and the sample can be varied in the range of 0.5 to 5 mm. Because the

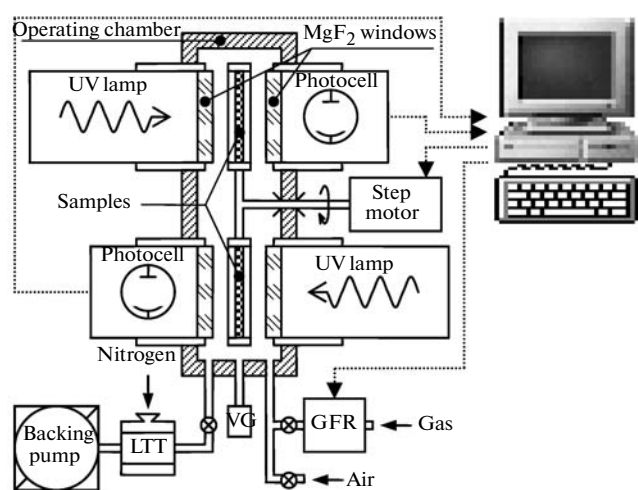


**Fig. 1.** Simplified functional scheme of the UPM-2 experimental system. LTT—low-temperature trap, VG—vacuum gauge, GFR—gas flowrate regulator. The distance between the sample and the lamp ranges from 0.5 to 5 mm.

PMS-2 system is designed to operate in a low vacuum (the minimum pressure is 2 Pa), this distance determines the efficiency of the VUV effect on a treated polymer surface. The smaller the distance, the higher the radiation intensity absorbed by the surface.

The PMS-2 system makes it possible to treat two sides of the polymer. After one side has been treated, the samples are interchanged by rotating the holder through  $180^\circ$  and the other side is then treated. Because the radiation intensity of the krypton lamp decreases with time, it is necessary to correct the exposure time periodically in order to provide a constant dose of sample irradiation. For this purpose, the sample holder is rotated through  $90^\circ$  at the command of a computer; after that, the radiation intensity of the lamp is measured by insensitive to visible light photocells having CuJ photocathodes and  $MgF_2$  detector windows (State Optical Institute).

The object under study was a poly(methyl methacrylate) ( $-\text{CH}_2-\text{C}(\text{CH}_3)-\text{COOCH}_3)_n$  film deposited on the polished Si(100) surface (KDB-10) by centrifuging (the speed of rotation was 1500 revolutions per minute and the duration was 2 min). In our experiments we used PMMA having viscosity-average molecular weight equal to  $7.7 \times 10^4$ . The film thickness was determined by using MII-4 microinterferometer (Leningrad Optical-Mechanical Amalgamation) and was approximately equal to  $0.8 \mu\text{m}$ . The studies were performed in a vacuum under residual pressures of 2 and 100 Pa. The samples were exposed to VUV radiation with durations of 0.5, 1, 2, 5, 10, and 20 min.

The photon energy of the KrR-3 krypton lamp is about 10 eV. This energy is sufficient to excite polymer molecules and break the chemical bonds C–C, C–H, and C–O [15]. During photolysis, the following compounds are formed: methyl formate  $\text{HCOOCH}_3$ , formalde-

hyde  $\text{CH}_2=\text{O}$ , methanol  $\text{CH}_3-\text{OH}$ , methyl methacrylate (MMA)  $\text{CH}_2=\text{C}(\text{CH}_3)-\text{COOCH}_3$ , and gaseous products such as  $\text{CO}$ ,  $\text{CO}_2$ ,  $\text{H}_2$ ,  $\text{H}_2\text{O}$ , and  $\text{CH}_4$  [15]. In addition, intermolecular linking occurs in film under VUV irradiation [15]. Thus, the observed effect of nanopography smoothing under VUV irradiation is a result of simultaneous action of the following processes: polymer photoetching, photostimulated oxidation, partial material redeposition, intermolecular linking formation, and mechanical surface relaxation. As shown below, the degree of smoothing mainly depends on the treatment time for a fixed radiation intensity and a residual air pressure in the working chamber ranging from 2 to 100 Pa.

Since the initial PMMA film (Fig. 2a) has a sufficiently smooth surface without any noticeable topographical features (the average roughness  $S = 1.1 \text{ nm}$ , see Table 1; even on an area of several squared millimeters, the surface roughness can be equal to several nanometers [17]), the UV irradiation smoothing effect cannot be revealed after the VUV treatment. Therefore, the initial PMMA film was nanostructured in nonequilibrium oxygen RF-plasma for 20 s.

The nanostructuring was performed using PCT-100T plasmochemical treatment system (Engineering Plant “Quartz”). The operating frequency of the RF generator was 13.56 MHz, and the plasma excitation was inductive. The leakage rate of high purity oxygen into the reactor chamber was about 30 l/h, the residual pressure ranged from 10 to 20 Pa, and the glow discharge power 500 W. Similar results were obtained for an oxygen RF plasma using a Plasma 600T plasmochemical treatment system (Research Institute of Semiconductor Engineering). The operating frequency of the RF generator was 13.56 MHz, and the plasma excitation was capacitive. The film was treated for 1 min under 40 Pa residual pressure of the working gas in the chamber, glow discharge power about 400 W, grid current 80 mA, and anode current 0.9 A.

As a result of PMMA film etching, nanograins with the lateral sizes about 66 nm, height about 1.8 nm, and distance between neighbour nanograins about 104 nm (mean values, see Table 2) are formed on the surface (Fig. 2b). The number of grains per unit area is approximately  $122 \mu\text{m}^{-2}$ . The technology used for nanostructuring provides a good reproducibility of results.

As in the case of VUV treatment, the polymer treatment in the oxygen RF-plasma changes only a thin near-surface layer of 1–10 nm thickness leaving a polymer in the bulk unaffected [17, 18]. The formation of nanograins can be explained by local variations in the PMMA film density and, accordingly, by the different etching rate [19]. The local density variations are related to the presence of inhomogeneities in the majority of polymers, first of all, grains (globules) [20–23], lamellas [20–23] as well as coiled molecules, bundles, nodes, twistings, tangles of molecular chains [23], etc.

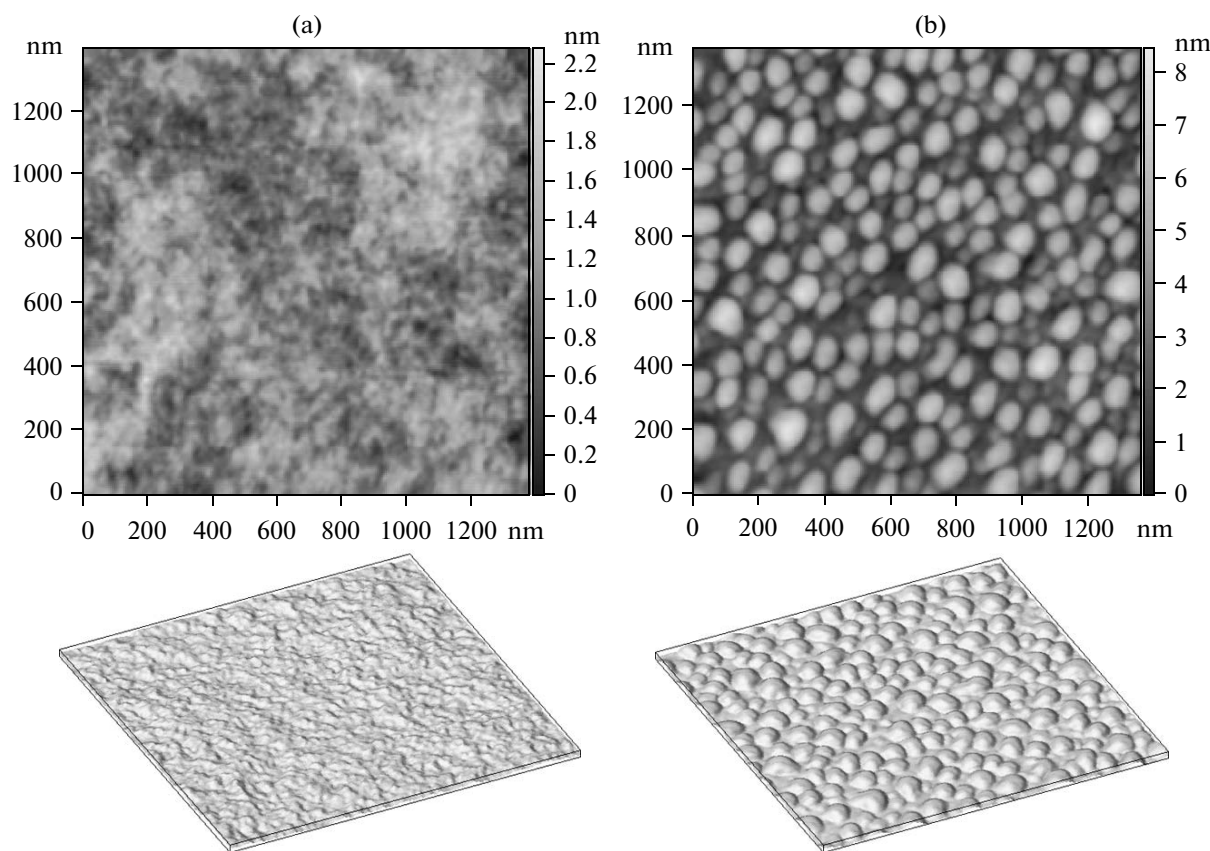


**Fig. 2.** AFM images of the PMMA film: (a) the initial surface after deposition on the Si substrate and (b) the nanostructured surface obtained as a result of the treatment of the initial surface in the oxygen radio-frequency plasma.

In addition to the change in the surface morphology, a considerable chemical modification of the polymer surface occurs during the PMMA treatment in oxygen plasma. In particular, polar functional groups as well as carbonate ( $O_2C=O$ ) and free carbonyl ( $C=O$ ) groups appear [17, 18]. The amount of oxygen in the near-surface layer increases substantially during the first seconds of the treatment, and then its growth

slows down; afterwards, oxygen penetrates into the material comparatively slowly [17].

The surface morphology of the PMMA film was studied by atomic-force microscopy (AFM). The measurements were conducted using Solver™ P4 device (NT-MDT) in tapping mode. The spring constant of the Si cantilever (Institute of Physical Problems named after F. V. Lukin) was about 12 N/m, and

**Table 1.** Roughness parameters of the initial PMMA film and the nanostructured PMMA film before and after VUV treatment

Parameters	Initial PMMA film	Nanostructured PMMA film	Nanostructured PMMA film after VUV treatment											
			2						100					
Residual air pressure, Pa	–	–	2						100					
Duration of VUV treatment $t$ , min	0	0	0.5	1	2	5	10	20	0.5	1	2	5	10	20
Peak-to-peak height $S_p$ , nm	2.2	8.6	9.3	7.0	5.8	4.2	2.4	2.4	7.7	7.5	7.4	5.6	2.7	2.3
Mean roughness $S$ , nm	1.1	3.4	2.9	3.0	1.9	2.0	1.1	1.2	2.4	2.8	2.5	2.1	1.3	1.1
Root-mean-square roughness $S_q$ , nm	0.26	1.36	1.10	0.91	0.67	0.43	0.26	0.27	0.91	0.98	0.81	0.52	0.29	0.25

**Table 2.** Geometric characteristics of features of the initial PMMA film and the nanostructured PMMA film before and after VUV treatment. The second value of the diameter corresponds to the lower estimate

Parameters	Initial PMMA film	Nanostructured PMMA film	Nanostructured PMMA film after VUV treatment											
	–	–	2						100					
Residual air pressure, Pa	–	–												
Duration of VUV treatment $t$ , min	0	0	0.5	1	2	5	10	20	0.5	1	2	5	10	20
Number of features $n$	424	214	320	278	275	320	314	395	202	214	243	192	225	335
Mean feature diameter $D$ , nm	30.5, 29.4	65.9, 50.2	51.8, 32.6	52.4, 40.2	52.9, 41.6	30.7, 29.0	32.9, 32.0	29.7, 28.6	59.7, 44.0	58.2, 44.3	54.9, 41.8	49.4, 45.6	37.1, 36.1	32.9, 31.9
Mean feature height $h$ , nm	0.13	1.8	2.2	1.4	1.3	0.20	0.10	0.13	1.8	1.6	1.5	0.44	0.12	0.12
Mean distance between features $d$ , nm	77.9	104.1	89.1	85.8	95.1	74.1	91.6	76.4	112.9	111.7	100.7	111.9	102.2	80.4

the resonant frequency was 130.800 kHz. The tip radius  $r$  of the cantilever probe did not exceed 10 nm.

To exclude the effect of spread of cantilever parameters on the scanning results, all measurements of the surface topography were made using one cantilever. In addition, the same scanning parameters were specified in all measurements; in particular, the same force was always applied to the surface. The force with which a cantilever presses on the soft polymer surface is a key parameter determining whether the relief under study is deformed or even damaged during the measurements [23].

Analysis of the roughness parameters [24, 25, 19] and geometrical sizes of the surface features (nanograins) of the PMMA film was conducted over  $1.4 \times 1.4 \mu\text{m}^2$  area. The geometrical sizes of the features were determined during computer topography recognition performed by feature-oriented scanning (FOS) method in the virtual mode [26]. In contrast to existing systems used to analyze features, such as grain analysis, in FOS method, a local horizontal cutting plane is drawn for each feature that makes it possible to determine feature parameters more precisely.

The typical size of the sample  $n$  was 200–400 features depending on VUV treatment time. The geometrical dimensions of the features are presented in the lateral plane by mean diameter  $D$  of a circle inscribed in the visible feature base and by mean height  $h$  in the vertical plane. In addition, the mean distance  $d$  between the neighboring features was calculated. The obtained data are given in Table 2.

Because the dimensions of the observed features are comparable with the radius of curvature  $r$  of the AFM probe tip, it is necessary to take into account a possible broadening of the lateral feature dimensions, in our case – the base diameter  $D$ . The value of the broadening was estimated by formula  $\Delta D = 2\sqrt{2rh - h^2}$

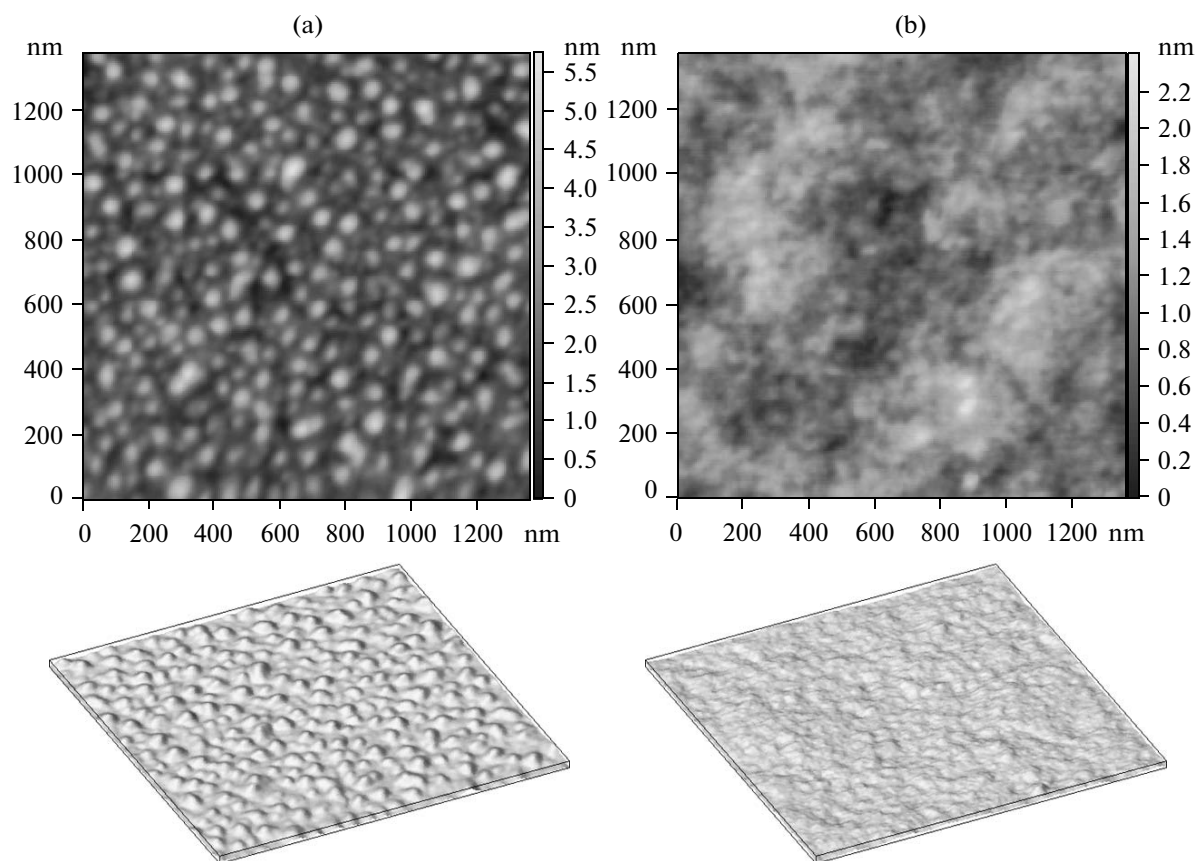
obtained from simple geometric considerations. Writing this formula, we assumed that the probe tip has the shape of a ball and the lateral feature surface is a vertical wall. The lower estimate of the feature diameter obtained by subtracting  $\Delta D$  from  $D$  is given in Table 2 after the comma. The true value of the feature diameter is somewhere between the measured value  $D$  and its lower estimate.

## RESULTS AND DISCUSSION

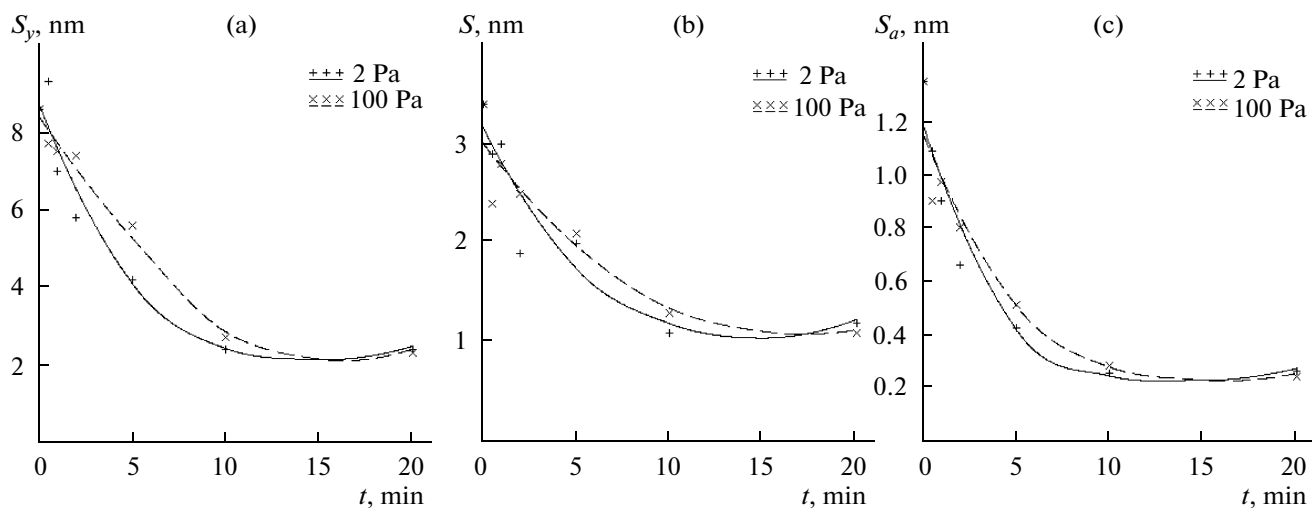
Figures 3a and 3b show surface images obtained as a result of 2 and 10 min VUV treatment of the nanostructured PMMA film under 2 Pa residual air pressure in the chamber. Here and hereafter, the surface images of the samples treated under a pressure of 100 Pa are not shown, because they are qualitatively similar to those of films treated under a pressure of 2 Pa. The number of points constituting the AFM images is  $256 \times 256$ . The roughness parameters of the obtained films are given in Table 1.

Figure 4 shows the data listed in Table 1 as dependences of peak-to-peak heights  $S_p$ , mean roughness  $S$ , and root-mean-square roughness  $S_a$  of the nanostructured PMMA surface on the VUV treatment time  $t$  under an air pressure of 2 and 100 Pa. Regression curves are drawn through the obtained experimental points using the least-squares method. Here and hereafter, the local regression (loess) was used to draw curves, because the third-order polynomial oscillated in the range of large times; a small “ski jump” at the end part of the curves is related to calculation peculiarities of the local regression.

The comparison of the roughness parameters of the samples treated under residual pressure 2 Pa with the parameters of the samples treated under residual pressure 100 Pa shows that these VUV treatment processes are approximately the same. At the beginning, the pro-



**Fig. 3.** AFM images of the nanostructured PMMA film subjected to VUV irradiation under 2 Pa residual air pressure in the chamber. Treatment time: (a) 2 min and (b) 10 min.



**Fig. 4.** Dependences of the roughness parameters (a)  $S_y$ , (b)  $S$ , and (c)  $S_a$  of the nanostructured PMMA film on the VUV treatment time  $t$  under 2 and 100 Pa air pressures in the working chamber.

cess of PMMA film irradiation under a higher residual air pressure of 100 Pa has smaller smoothing rate and, correspondingly, changes the nanostructured surface of the PMMA film to a smaller extent (Fig. 4). Probably, the small rate of smoothing is related to an addi-

tional absorption of VUV radiation. The smoothing rates become the same after approximately five minutes of treatment, then the smoothing rate under 2 Pa pressure decreases faster than that under 100 Pa pressure. In the latter case, the change in the rate is prob-

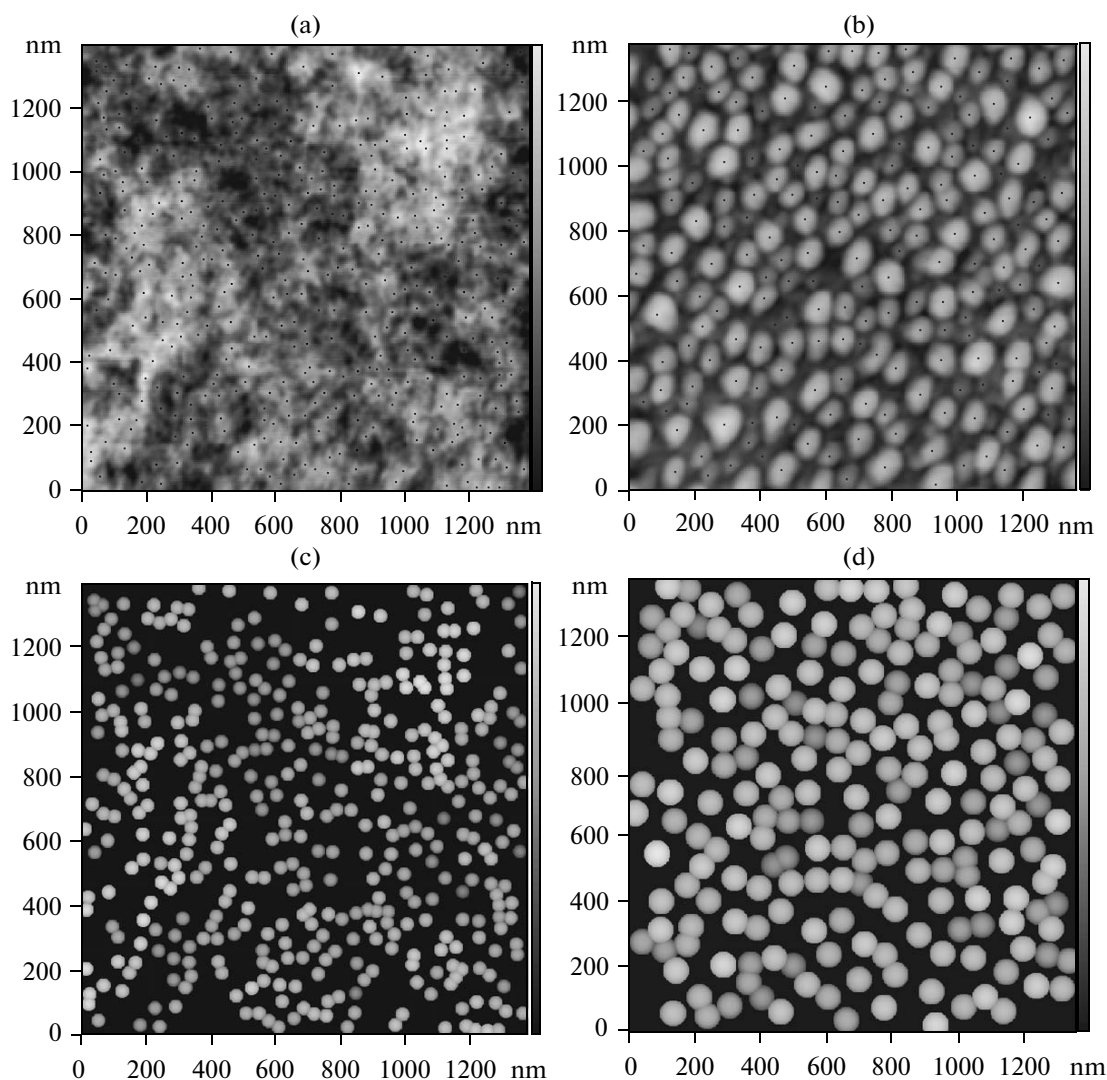


**Fig. 5.** Specific surface features recognized in the image of the (a) initial and (b) nanostructured PMMA film during the virtual FOS. The position of the point corresponds to the center of gravity of the visible base of the recognized feature. For the real surface images (a) and (b), the schematic representations (c) and (d) were built in which the features are imaged as hemispheres.

ably related to a change in the ratio of the components forming the gas mixture. Finally, after the 15 min treatment, the smoothing rates of both processes decrease to zero, and the roughness obtained becomes the same as that of the initial film. Thus, after 15 minutes of the VUV treatment, irrespective of the pressure in the working chamber, the dynamic equilibrium state had happened, at which the processes of the photo-etching and partial redeposition would not change the surface roughness.

Results of analysis of the PMMA surfaces by FOS method are shown in Figs. 5 and 6. Application of FOS enables us to find surface features (nanograins in our case) and determine their main geometrical characteristics (see Table 2) in automatic mode. The advantage of the FOS method is that it makes possible to discover features in such images where they are almost unnoticeable by eye. For example, this method

can detect features having small lateral sizes (see Figs. 5a, 6b), small heights, complicated base shape, and also those located on a strongly developed underlying topography.

Figures 5c, 5d, 6c, and 6d show images of the obtained surfaces in the schematic form, which simplifies their analysis. In particular, using the schematic (model) representation makes possible to better understand the surface structure. This representation is especially useful while analyzing surfaces, which consist of a large number of small, weakly distinguishable features (see Figs. 5a, 6b).

Based on the data presented in Table 2, the dependences of nanograin number, mean nanograin diameter, mean nanograin height, and mean distance between the neighbour nanograins on VUV irradiation time  $t$  under 2 and 100 Pa air pressure in the working chamber are built (see Fig. 7). On the whole, the anal-

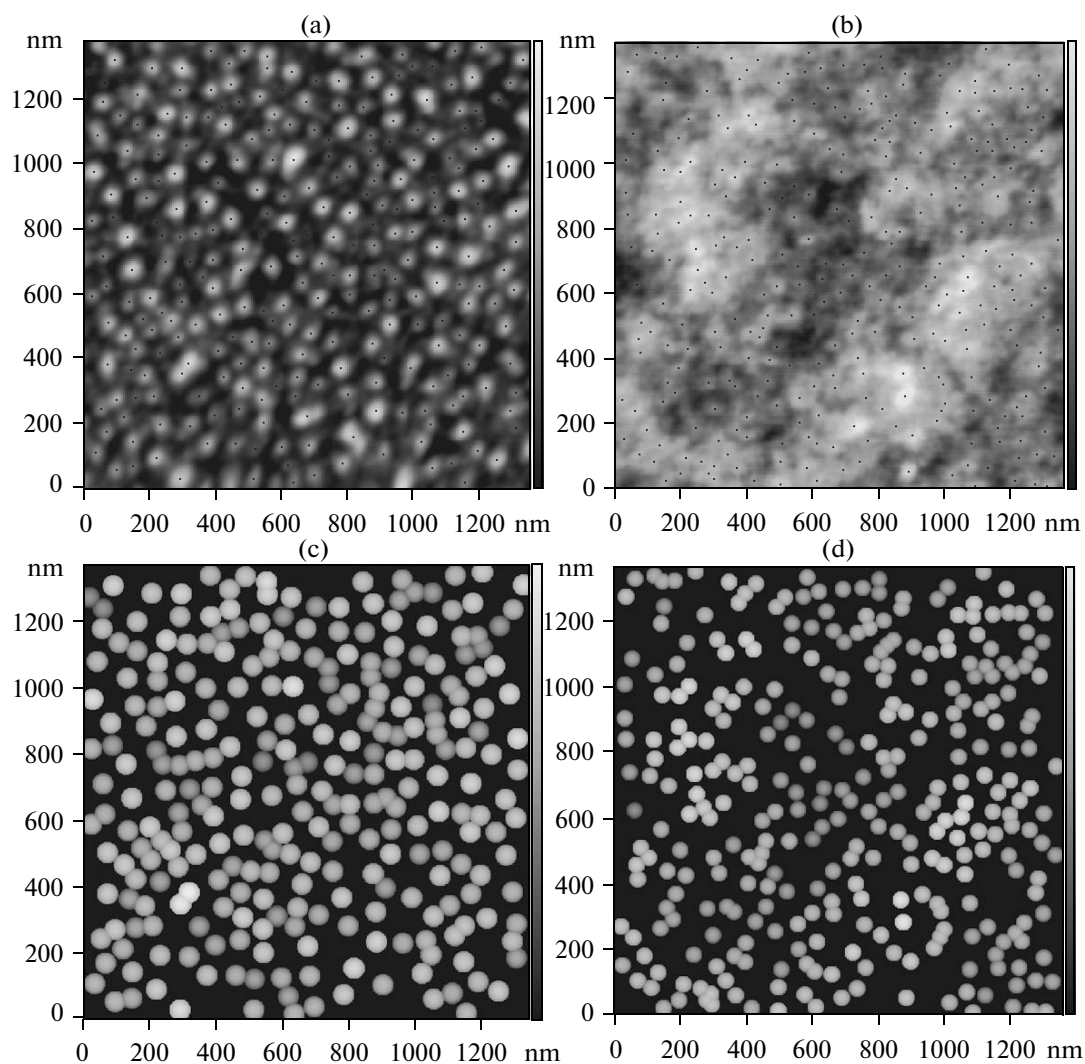


**Fig. 6.** Specific surface features recognized in the image of the nanostructured PMMA film exposed to VUV irradiation under 2 Pa pressure for (a) 2 and (b) 10 min. The images (c) and (d) are schematic representations of the images (a) and (b), respectively.

ysis of the obtained results shows that smoothing of the features of the nanostructured surface of the PMMA film is well noticeable even after 2 minutes of VUV irradiation (see Fig. 3a, compare with Fig. 2b). After 10 minutes of VUV irradiation, the value of mean roughness decreases by a factor of 2.6–3 (Table 1, Fig. 4), mean lateral size of nanograins decreases two-fold, and mean nanograin height decreases by a factor of 15–18 (Table 2, Figs. 7b, 7c). Thus, after 10 minutes of the VUV exposure, the obtained surface becomes comparable with the smooth surface of the initial PMMA film obtained on the centrifuge (see Fig. 3b, compare with Fig. 2a).

The comparison of the curves in Figs. 7a and 7d shows that occurrence of new surface features and decrease of a mean distance between surface features during interaction of UV radiation with the polymer in the presence of oxygen are two mutually opposite processes. Hence, we can conclude that gaseous photoly-

sis products redeposit under VUV irradiation, because PMMA film etching in the oxygen plasma leads to the opposite result, namely, to a noticeable decrease in the number of features and to an increase in the distance between them (Table 2).

It should be noted that the experimental values given in Figs. 7a and 7d have a strong spread. This means that some local subprocesses occur in the chosen time ranges. Thus, the regression curves show only a general character of a sufficiently complicated process of the VUV treatment in this case. For this reason, in contrast to the other curves, these curves have no horizontal regions of saturation after 10–15 minutes of film treatment.

Analysis of the images in Figs. 5 and 6 allows detecting sequences forming linear and slightly curved chains among the chaotically scattered features [22]. The features forming these structures have approximately the same dimensions and are located at

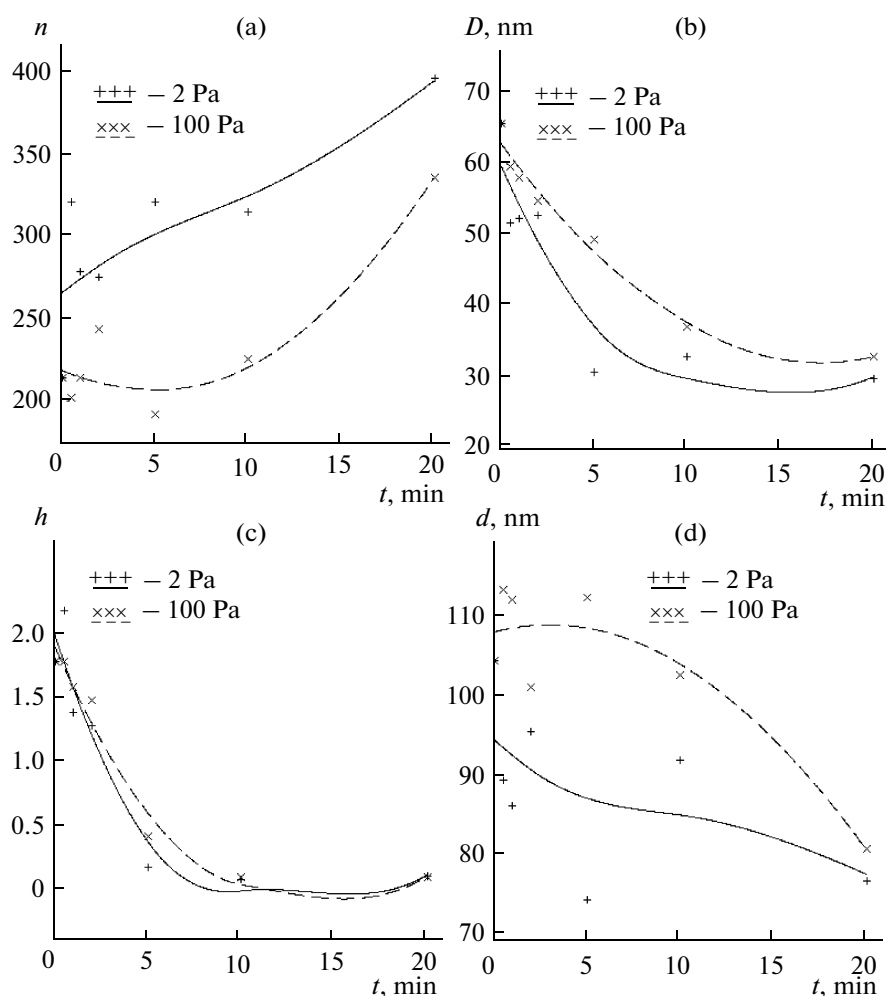


**Fig. 7.** Dependences of (a) number  $n$  of features, (b) mean base diameter  $D$ , (c) mean feature height  $h$ , and (d) mean distance  $d$  between neighbour features of the nanostructured PMMA film on VUV treatment time  $t$  under 2 and 100 Pa air pressures in the working chamber.

approximately the same distance (35–80 nm) from each other. The chain can consist of two, three, four and more nanograins. The indicated chains exist both on the initial PMMA film and on PMMA films treated in the oxygen plasma and exposed to VUV radiation. The discovered chains probably are a part of the polymer film structure. The chains on the initial surface are short and randomly oriented. It is possible that the short chains observed on the initial surface are a part of longer chains going into bulk of the material.

The revealed structure is seen especially clear on the film treated in the oxygen plasma (Fig. 5b). Here, the chains contain a large number of elements with approximately the same dimensions located at approximately the same distance between each other; the chains have a small curvature and are oriented along a certain direction. Two directions on the surface along which the chain elements are mainly oriented can be distinguished. Approximately these directions are oriented along the diagonals of the given images.

Thus, the observed features and their mutual arrangement enable us to speak about a certain degree of two-dimensional ordering of the surface under consideration [20].

To confirm the periodical arrangement of the features on the PMMA film, the Fourier spectra of the surfaces under investigation were obtained (Fig. 8). The constant component, which yields small information in the analysis of spatial frequencies, was discarded (it corresponds to the mean roughness  $S$  numerically, see Table 1). The frequencies forming a “cross” at the spectrum center are related to the Fourier transformation method itself (they are induced by the edge effect); therefore, these frequencies should be simply ignored.

The data given in Fig. 8a demonstrate that the initial PMMA film produced by centrifuging contains no distinct peaks that could be associated with any (one- or two-dimensional) surface ordering. The spectrum

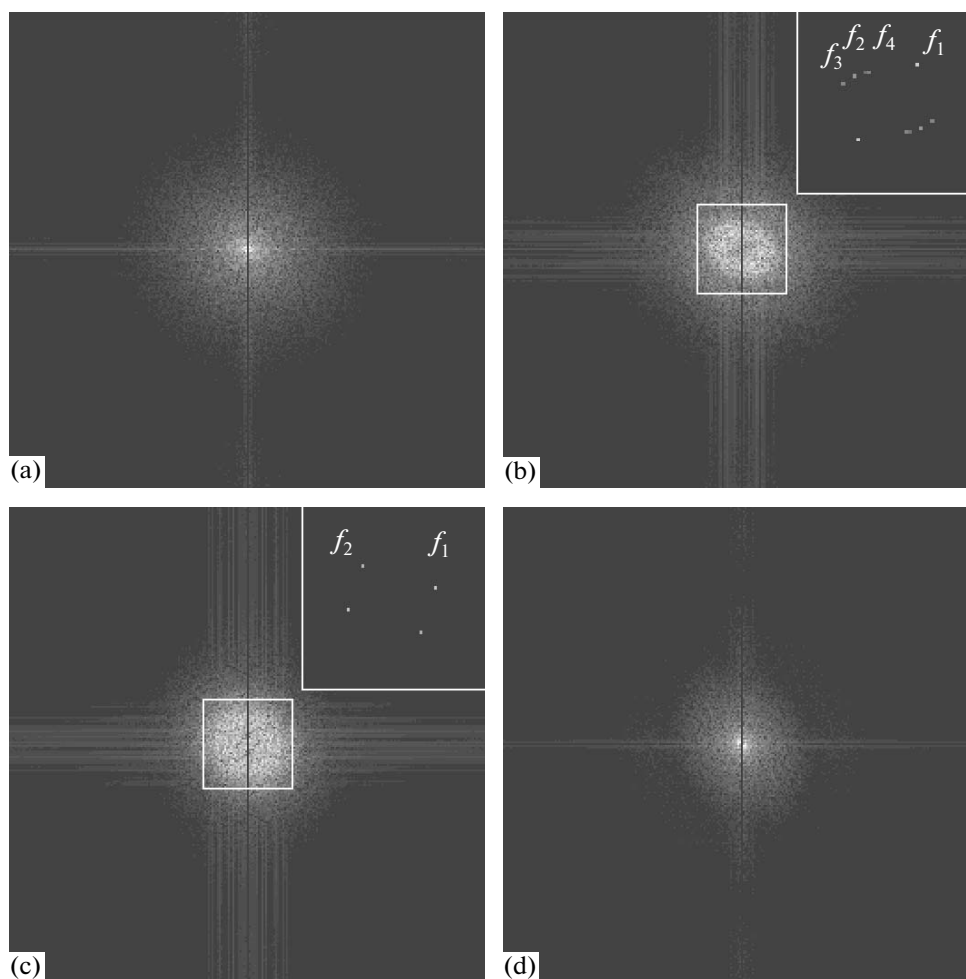


**Fig. 8.** Fourier spectra of the surface of the (a) initial PMMA film, (b) PMMA film nanostructured in the oxygen plasma, (c) nanostructured PMMA film after 2 min of VUV treatment under 2 Pa pressure, and (d) nanostructured PMMA film after 10 min of VUV treatment under 2 Pa pressure.

contains image components at all frequencies with the usually observed tendency toward a decrease in the amplitudes of harmonic components as the spatial frequency increases.

Figure 8b shows the Fourier spectrum of the PMMA film surface nanostructured in the oxygen plasma. The insert in Fig. 8b contains only peaks that differ noticeably from the others. There are four such peaks. The following spatial frequencies correspond to the found peaks:  $f_1 = 1/107.1 \text{ nm}^{-1}$ ,  $f_2 = 1/120.0 \text{ nm}^{-1}$ ,  $f_3 = 1/105.0 \text{ nm}^{-1}$ , and  $f_4 = 1/145.5 \text{ nm}^{-1}$ . The frequencies are given in descending order of their amplitudes (arbitrary units): 27.1, 25.0, 23.9, and 23.8, respectively.

Other harmonics in the low-frequency region of the spectrum, where the main information on the images is usually concentrated, were rejected as less significant for our analysis. Four selected peaks are slightly distinguished on the spectrum, because a nonlinear scale (a logarithmic one) was used for spectrum rendering. The nonlinear scale is required for visual-

ization of the whole spectrum, in particular, for imaging the response related to high frequencies.

It should immediately be mentioned that the spatial period  $1/f_1 = 107.1 \text{ nm}$  extracted from the spectrum agrees well with the mean distance  $d = 104.1 \text{ nm}$  between the features, which was determined during the virtual FOS. The harmonic oscillation with the frequency  $f_1$  propagates along the direction making angle  $51.1^\circ$  with the  $x$  axis. The harmonic oscillation with the frequency  $f_2$  propagates almost perpendicularly ( $91.3^\circ$ ) to the oscillation with the frequency  $f_1$ . Both of these facts confirm the previously discovered orientation of the grain chains along the image diagonals (Figs. 2b, 5b).

The propagation directions of the oscillations  $f_3$  and  $f_4$  make respective angles of  $+15.0^\circ$  and  $-25.5^\circ$  with the direction of the oscillations with the frequency  $f_2$ ; moreover, both oscillations have almost the same amplitudes. The harmonic oscillations  $f_3$  and  $f_4$  are probably satellites of the oscillation  $f_2$ ; i.e., they are

some deviations from the direction of this oscillation. The discovered deviations are probably associated with the structure of the PMMA macromolecule and with peculiarities of its interaction with the neighboring macromolecules. Thus, the detection of the frequencies  $f_1$  and  $f_2$  demonstrates directly that the nanostructured surface of the PMMA film has a certain two-dimensional order [20].

A portion of the spectrum contained in the square has the oval shape meaning that the observed grain in the image plane also has, on average, the oval shape. Furthermore, the long oval axis coincides almost with the propagation direction of the harmonics  $f_3$ , which corresponds to the flattened shapes of grains along this direction (Figs. 2b, 5b). A deficiency of low frequencies, whose reciprocals are comparable with the sizes of the considered image, is observed in the spectrum center. Such deficiency indicates that after PMMA etching in the oxygen plasma, the surface in the above mentioned scale became flatter than the initial one, despite of the grain formation caused a local fourfold increase in height difference. Thus, the in-depth etching process while nanostructuring develops evenly over 0.3–1.4  $\mu\text{m}$  regions, the etching unevenness reveals itself only locally in the form of grain formation.

Figure 8c shows the Fourier spectrum of the nanostructured surface of the PMMA film treated in VUV during 2 min under 2 Pa pressure. Two characteristic frequencies  $f_1 = 1/110.3 \text{ nm}^{-1}$  and  $f_2 = 1/113.8 \text{ nm}^{-1}$  with amplitudes 11.2 and 9.6, respectively, can be found in the spectrum. The presence of the frequencies  $f_1$  and  $f_2$  shows that surface features still form the two-dimensional partially ordered structure. The frequencies-satellites  $f_3$  and  $f_4$  observed before VUV treatment vanished; in addition, the amplitudes of the harmonic oscillations with the frequencies  $f_1$  and  $f_2$  decreased by a factor of 2.5. The frequencies  $f_1$  and  $f_2$  differ in Fig. 8c to a smaller extent than those in Fig. 8b; consequently, some sort of equalization of the spatial periodicity along the selected directions took place during the VUV treatment.

It is also worth paying attention to the fact that the deficiency of low frequencies observed in the preceding spectrum turns out to be made up. Despite this, the image relief did not become noticeably less flatter in the scale comparable with the scan size because of small amplitude of these low frequencies. An increase in the number of high frequencies inside the region denoted by the square indicates a decrease in the feature diameter. The spectrum inside square does not longer have an oval shape meaning that the lateral cross sections of the grains became circular.

Figure 8d shows the Fourier spectrum of the surface of the nanostructured PMMA film treated in VUV during 10 min under 2 Pa pressure. The spectrum contains no frequencies related to any periodic structure. On the whole, the spectrum corresponds to that of the initial PMMA film (Fig. 8a) obtained by centrifuging.

## CONCLUSIONS

Our studies showed that using the VUV treatment with the radiation wavelength  $\lambda = 123.6 \text{ nm}$  and intensity around  $7 \text{ mJ cm}^{-2} \text{ s}^{-1}$  allows to change the film thickness and the roughness of the PMMA surface quite effectively in the nanometer range. In particular, by subjecting the nanostructured PMMA surface having mean feature height 1.8 nm to UV radiation during 10 min under 2–100 Pa residual air pressure in the working chamber, it is possible to obtain the surface roughness comparable to that of the initial smooth film (a mean feature height of about 0.1 nm) deposited on a polished substrate by centrifuging.

The nanostructured surface of the PMMA film during VUV treatment under a low air pressure is smoothed as a result of the simultaneous action of two opposite processes, namely, polymer photodissociation and photostimulated oxidation, on the one hand, and partial redeposition and intermolecular linking, on the other hand [15]. Moreover, the mechanical relaxation of the film surface stimulated by radiation defects occurs. Redeposited photolysis products fill the space between the nanostructured surface grains subjected to oxidation and etching. As a result, the relief of the film surface after the VUV treatment approaches to the initial sample with the smooth surface typical of PMMA having no any features or structure. To accelerate the process and improve reproducibility, the air supplied in the chamber can be replaced with high-purity oxygen.

The Fourier spectrum of spatial frequencies of the PMMA film nanostructured in the oxygen plasma unambiguously demonstrates the presence of the two-dimensional quasiperiodic structure, which is a system of parallel chains of nanograins. The nanograins themselves are probably polymer globules. The partially ordered surface nanostructure was completely disintegrated during the subsequent VUV treatment that finds its confirmation in the corresponding Fourier spectra.

The nature of the discovered ordering is now studied. In particular, it is necessary to understand whether the nanograins and the partially ordered structure were formed during the PMMA film treatment in oxygen plasma or during polymerization [20–22] and were then simply “decorated” on the surface of the initial film with mobile polymer fragments of lower molecular mass [22]. In addition, a relationship between surface roughness, processes of surface chemical modification in oxygen plasma and in VUV, and surface hydrophobic properties [17, 19] is planned to be investigated; in particular, this is important for “adjusting” biocompatibility parameters of surfaces of PMMA implants [14].

The nanostructured surface of PMMA resist exposed during electron-beam, UV, or X-ray lithography can be used as a mask after development to form partially ordered patterns of nanodots, nanocolumns, nanopores, etc. [20, 21]. In this case, the mask is pro-

duced, because, under the action of an electron beam, UV, or X-ray radiation, the degree of resist polymerization in nanograins will differ from that in the regions between the nanograins, and, accordingly, the resist solubility in these places will be different.

PMMA film nanostructured in oxygen plasma can also be used as a test surface for performance estimation of a nanotechnological equipment incorporating UV radiation sources.

#### ACKNOWLEDGMENTS

This work was supported by the Russian Foundation for Basic Research (grants no. 05-03-32394, no. 10-07-00173, no. 10-03-00792).

The authors are grateful to A.V. Novozhilov for preparation of the PMMA film, V.K. Belyi for treatment of the PMMA film in the oxygen plasma, and S.A. Bulgakova for critical reading of the manuscript.

#### REFERENCES

1. H. H. Solak, *J. Phys. D.* **39**, R171 (2006).
2. E. Dubois and J.-L. Bubbendorff, *Solid-State Electron.* **43**, 1085 (1999).
3. J. Hartwich, L. Dreeskornfeld, V. Heisig, et al., *Appl. Phys. A* **66**, S685 (1998).
4. L. J. Guo, *J. Phys. D.* **37**, R123 (2004).
5. F. Zhang and H. Y. Low, *Nanotechnology* **17**, 1884 (2006).
6. K.-S. Kim, Y. Ando, and K.-W. Kim, *Nanotechnology* **19**, 105701 (2008).
7. Y. Guo, G. Liu, Y. Xiong, and Y. Tian, *J. Micromech. Microeng.* **17**, 9 (2007).
8. J. M. Li, C. Liu, X. D. Dai, et al., *J. Micromech. Microeng.* **18**, 095021 (2008).
9. M. Haiducu, M. Rahbar, I. G. Foulds, et al., *J. Micromech. Microeng.* **18**, 115029 (2008).
10. S. E. Peltek, T. N. Goryachkovskaya, V. M. Popik, et al., *Nanotechnologies in Russia* **3**, No. 9-10, 622 (2008).
11. S. W. Li, J. H. Xu, Y. J. Wang, et al., *J. Micromech. Microeng.* **19**, 015035 (2009).
12. M. E. Vlachopoulou, A. Tserepi, P. Pavli, et al., *J. Micromech. Microeng.* **19**, 015007 (2009).
13. A. Nisar, N. Afzulpurkar, B. Mahaisavariya, and A. Tuantranont, *Sensors & Transducers* **94**, 176 (2008).
14. N. Gomathi, A. Sureshkumar, and S. Neogi, *Current Sci.* **94**, 1478 (2008).
15. K. A. Valiev, L. V. Velikov, Yu. I. Dorofeev, et al., *Poverkhnost: Fiz. Khim. Mekh.*, No. 6, 86 (1985) [in Russian].
16. C. Peth, F. Barkusky, and K. Mann, *J. Phys. D.* **41**, 105202 (2008).
17. J. Chai, F. Lu, B. Li, and D. Y. Kwok, *Langmuir* **20**, 10919 (2004).
18. H. Lim, Y. Lee, S. Han, et al., *J. Vac. Sci. Technol. A* **19**, 1490 (2001).
19. N. Vourdas, A. Tserepi, and E. Gogolides, *Nanotechnology* **18**, 125304 (2007).
20. S. Yoshida, T. Ono, and M. Esashi, *Nanotechnology* **19**, 475302 (2008).
21. D. K. Singh, R. V. Krotkov, H. Xiang, et al., *Nanotechnology* **19**, 245305 (2008).
22. J. H. Choi, S. M. Adams, and R. Ragan, *Nanotechnology* **20**, 065301 (2009).
23. S. Magonov and Y. Godovsky, *Am. Lab.* **31**, 52 (1999).
24. J. F. Jorgensen, K. Carneiro, and L. L. Madsen, *Nanotechnology* **4**, 152 (1993).
25. Ya. A. Rudzit and V. N. Plutalov, in *Principles of Metrology, Precision and Reliability in Instrument Design* (Mashinostroenie, Moscow, 1991) [in Russian].
26. R. V. Lapshin, *Nanotechnology* **15**, 1135 (2004) [available at [www.niifp.ru/staff/lapshin/en/](http://www.niifp.ru/staff/lapshin/en/)].